HAL open science

Improved formulation for the stabilized enhanced strain solid-shell element (SHB8PS): geometric linear and nonlinear applications

Farid Abed-Meraim, Alain Combescure

▶ **To cite this version:**

Farid Abed-Meraim, Alain Combescure. Improved formulation for the stabilized enhanced strain solid-shell element (SHB8PS): geometric linear and nonlinear applications. 17th International Conference on Computer Methods in Mechanics, Jun 2007, Lodz-Spala, Poland. 9 pp. hal-01226198

HAL Id: hal-01226198

https://hal.science/hal-01226198v1

Submitted on 9 Feb 2022

HAL is a multi-disciplinary open access archive for the deposit and dissemination of scientific research documents, whether they are published or not. The documents may come from teaching and research institutions in France or abroad, or from public or private research centers.

L'archive ouverte pluridisciplinaire **HAL**, est destinée au dépôt et à la diffusion de documents scientifiques de niveau recherche, publiés ou non, émanant des établissements d'enseignement et de recherche français ou étrangers, des laboratoires publics ou privés.

Distributed under a Creative Commons Attribution - NonCommercial 4.0 International License

Improved formulation for the stabilized enhanced strain solid-shell element (SHB8PS): geometric linear and nonlinear applications

Farid Abed-Meraim[+] and Alain Combescure[*]
[+] *LPMM UMR CNRS 7554, ENSAM CER de Metz, 4 rue Augustin Fresnel, 57078 Metz, France*
[*] *LaMCoS UMR CNRS 5514, INSA de Lyon, 18, 20 rue des Sciences, 69621 Villeurbanne, France*
e-mail: farid.abed-meraim@metz.ensam.fr

Abstract

In this study, the formulation of the SHB8PS solid-shell element is reviewed in order to eliminate some persistent membrane and shear locking phenomena. The resulting physically stabilized and locking-free finite element consists in a continuum mechanics shell element based on a purely three-dimensional formulation. In fact, this is a hexahedral element with eight nodes as well as five integration points, all distributed along the "thickness" direction. Consequently, it can be used for the modelling of thin structures, while providing an accurate description of the various through-thickness phenomena. The reduced integration has been used in order to prevent some locking phenomena and to increase computational efficiency. The spurious zero-energy deformation modes due to the reduced integration are efficiently stabilized, whereas the strain components corresponding to locking modes are eliminated with a projection technique following the Enhanced Assumed Strain (EAS) method.

Keywords: SHB8PS solid-shell element, hourglass, locking, Enhanced Assumed Strain

1. Introduction

Over the last decade, considerable progress has been made in the development of three-dimensional finite elements capable of modelling thin structures (see Refs. [1], [2], [5], [10], [16]). This interest is motivated by several requirements that can be met in certain industrial applications. Indeed, the coupling between solid and shell formulations is a good way to provide continuum finite element models that can be efficiently used for structural applications. The SHB8PS element is one such recently developed element, based on a purely three-dimensional formulation (see Refs. [1], [2], [10]). This solid-shell element has numerous advantages for the analysis of various complex structural forms that are common in many industrial applications. Its main advantage is to allow the meshing of complex structural forms without the classical problems of connecting zones meshed with different element types (continuum and structural elements for instance). Another important benefit of solid-shell elements is the avoidance of tedious and complex pure-shell element formulations.

In this work, a new locking-free formulation for the SHB8PS solid-shell element is developed. More specifically, this work focuses on the elimination of the residual membrane and shear locking phenomena persisting in the previous formulations. By using orthogonal projection of the discretized gradient operator, these severe shear and membrane locking modes are removed. Moreover, reduced integration is used in order to improve the computational efficiency of the element and also to prevent some membrane and shear locking phenomena. The spurious zero-energy deformation modes due to this reduced integration are efficiently controlled by a stabilization technique following the approach given in Ref. [3]. To assess the effectiveness of this new version of the SHB8PS, several numerical experiments were performed. A selected set of these popular test problems is presented in this paper. It is shown that in many linear and nonlinear well-known benchmark problems, this new formulation of the SHB8PS element proves to be free of locking phenomenon and exhibits good convergence properties.

2. Formulation of the SHB8PS element

2.1. Kinematics and interpolation

SHB8PS is a hexahedral, eight-node and isoparametric element with linear interpolation. Its five integration points are spread along the ζ direction in the local coordinates. Figure 1 shows the reference geometry of the element as well as the location of the integration points.

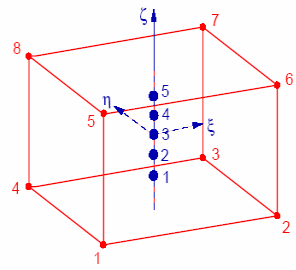

Figure 1: Reference geometry of the element and Gauss points.

The coordinates x_i, i = 1, 2, 3 of a point in the element are related to the nodal coordinates x_{iI} using the classical linear isoparametric shape functions N_I (I = 1, …, 8) and the relations:

$$x_i = x_{iI} N_I(\xi,\eta,\zeta) = \sum_{I=1}^{8} x_{iI} N_I(\xi,\eta,\zeta) \tag{1}$$

The convention of implied summation for repeated subscripts will be used hereafter, unless specified otherwise. The lowercase subscripts i go from one to three and represent the directions of the spatial coordinates. The uppercase ones I go from one to eight and correspond to the nodes of the element. With this convention, the interpolation of the

displacement field u_i inside the element in terms of the nodal displacements u_{iI} is similar:

$$u_i = u_{iI} N_I(\xi, \eta, \zeta) \tag{2}$$

2.2. Discrete gradient operator

The displacement field interpolation, Eqn. (2), allows the strain field to be related to the nodal displacements. The linear part of the strain tensor is written:

$$\varepsilon_{ij} = \frac{1}{2}\left(u_{i,j} + u_{j,i}\right) = \frac{1}{2}\left(u_{iI} N_{I,j} + u_{jI} N_{I,i}\right) \tag{3}$$

Then, the classical tri-linear shape functions for eight-node hexahedral elements are considered:

$$\begin{aligned} &N_I(\xi, \eta, \zeta) = \frac{1}{8}(1+\xi_I \xi)(1+\eta_I \eta)(1+\zeta_I \zeta) \\ &\xi, \eta, \zeta \in [-1, 1],\ I = 1,...,8 \end{aligned} \tag{4}$$

Combining Eqns. (1), (2) and (4), leads to the expansion of the displacement field as a constant term, linear terms in x_i and some terms depending on the h_α functions:

$$\begin{cases} u_i = a_{0i} + a_{1i} x + a_{2i} y + a_{3i} z + c_{1i} h_1 + c_{2i} h_2 + c_{3i} h_3 + c_{4i} h_4 \\ i = 1, 2, 3 \\ h_1 = \eta\zeta,\ h_2 = \zeta\xi,\ h_3 = \xi\eta,\ h_4 = \xi\eta\zeta \end{cases} \tag{5}$$

When this equation is evaluated at the element nodes, the three systems of eight equations are obtained as seen below:

$$\begin{cases} \underline{d}_i = a_{0i} \underline{s} + a_{1i} \underline{x}_1 + a_{2i} \underline{x}_2 + a_{3i} \underline{x}_3 + c_{1i} \underline{h}_1 + c_{2i} \underline{h}_2 + c_{3i} \underline{h}_3 + c_{4i} \underline{h}_4 \\ i = 1, 2, 3 \end{cases} \tag{6}$$

In the equation above, the $\underline{d}_i$ and $\underline{x}_i$ vectors respectively indicate the nodal displacements and coordinates and are defined as:

$$\begin{cases} \underline{d}_i^T = (u_{i1}, u_{i2}, u_{i3}, ..., u_{i8}) \\ \underline{x}_i^T = (x_{i1}, x_{i2}, x_{i3}, ..., x_{i8}) \end{cases} \tag{7}$$

The vectors $\underline{s}$ and $\underline{h}_\alpha$ $(\alpha = 1, ..., 4)$ are given by:

$$\begin{cases} \underline{s}^T = (1,1,1,1,1,1,1,1) \\ \underline{h}_1^T = (1,1,-1,-1,-1,-1,1,1) \\ \underline{h}_2^T = (1,-1,-1,1,-1,1,1,-1) \\ \underline{h}_3^T = (1,-1,1,-1,1,-1,1,-1) \\ \underline{h}_4^T = (-1,1,-1,1,1,-1,1,-1) \end{cases} \tag{8}$$

The unknown constants a_{ji} and $c_{\alpha i}$ in Eqn. (5) are found by introducing the $\underline{b}_i$ $(i = 1,..., 3)$ vectors from Ref. [7], defined as:

$$\underline{b}_i^T = \underline{N}_{,i}(0,0,0) \qquad i = 1,2,3 \qquad \textit{Hallquist Form} \tag{9}$$

The explicit expressions for the derivatives of the shape functions evaluated at the origin of the (ξ, η, ζ) frame are given in Ref. [4]. The following orthogonality properties are first demonstrated, implying the vectors $\underline{b}_i$ and the vectors $\underline{x}_i^T = (x_{i1}, x_{i2}, ..., x_{i8})$, $\underline{d}_i^T = (u_{i1}, u_{i2}, ..., u_{i8})$, $\underline{s}$, $\underline{h}_1$, $\underline{h}_2$, $\underline{h}_3$, $\underline{h}_4$:

$$\begin{cases} \underline{b}_i^T \cdot \underline{h}_\alpha = 0 \quad , \quad \underline{b}_i^T \cdot \underline{s} = 0 \quad , \quad \underline{b}_i^T \cdot \underline{x}_j = \delta_{ij} \\ \underline{h}_\alpha^T \cdot \underline{s} = 0 \quad , \quad \underline{h}_\alpha^T \cdot \underline{h}_\beta = 8\delta_{\alpha\beta} \\ i, j = 1, ..., 3 \qquad \alpha, \beta = 1,...,4 \end{cases} \tag{10}$$

In order to calculate the constants a_{ji} and $c_{\alpha i}$, Eqn. (6) is multiplied by $\underline{b}_i^T$ and $\underline{h}_\alpha^T$, respectively. Then, using the previously derived orthogonality conditions, one obtains:

$$\begin{cases} a_{ji} = \underline{b}_j^T \cdot \underline{d}_i \quad , \quad c_{\alpha i} = \underline{\gamma}_\alpha^T \cdot \underline{d}_i \\ \text{where: } \underline{\gamma}_\alpha = \dfrac{1}{8}\left[\underline{h}_\alpha - \sum_{j=1}^{3} (\underline{h}_\alpha^T \cdot \underline{x}_j)\underline{b}_j\right] \end{cases} \tag{11}$$

The displacement field can be expressed in the following form, very convenient for the subsequent developments:

$$u_i = a_{0i} + (x_1 \underline{b}_1^T + x_2 \underline{b}_2^T + x_3 \underline{b}_3^T + h_1 \underline{\gamma}_1^T + h_2 \underline{\gamma}_2^T + h_3 \underline{\gamma}_3^T + h_4 \underline{\gamma}_4^T) \cdot \underline{d}_i \tag{12}$$

By differentiating this last equation with respect to x_j, one obtains the displacement gradient as follows:

$$u_{i,j} = \left(\underline{b}_j^T + \sum_{\alpha=1}^{4} h_{\alpha,j} \underline{\gamma}_\alpha^T\right) \cdot \underline{d}_i = \left(\underline{b}_j^T + h_{\alpha,j} \underline{\gamma}_\alpha^T\right) \cdot \underline{d}_i \tag{13}$$

This allows us to express the discrete gradient operator, relating the strain field to the nodal displacements, as:

$$\underline{\underline{\nabla}}_s(\underline{u}) = \underline{\underline{B}} \cdot \underline{d}$$

$$\text{where:} \quad \underline{\underline{\nabla}}_s(\underline{u}) = \begin{bmatrix} u_{x,x} \\ u_{y,y} \\ u_{z,z} \\ u_{x,y} + u_{y,x} \\ u_{y,z} + u_{z,y} \\ u_{x,z} + u_{z,x} \end{bmatrix} \quad , \quad \underline{d} = \begin{bmatrix} \underline{d}_x \\ \underline{d}_y \\ \underline{d}_z \end{bmatrix} \tag{14}$$

This discrete gradient operator finally takes the following practical matrix form:

$$\underline{\underline{B}} = \begin{bmatrix} \underline{b}_x^T + h_{\alpha,x} \underline{\gamma}_\alpha^T & \underline{0} & \underline{0} \\ \underline{0} & \underline{b}_y^T + h_{\alpha,y} \underline{\gamma}_\alpha^T & \underline{0} \\ \underline{0} & \underline{0} & \underline{b}_z^T + h_{\alpha,z} \underline{\gamma}_\alpha^T \\ \underline{b}_y^T + h_{\alpha,y} \underline{\gamma}_\alpha^T & \underline{b}_x^T + h_{\alpha,x} \underline{\gamma}_\alpha^T & \underline{0} \\ \underline{0} & \underline{b}_z^T + h_{\alpha,z} \underline{\gamma}_\alpha^T & \underline{b}_y^T + h_{\alpha,y} \underline{\gamma}_\alpha^T \\ \underline{b}_z^T + h_{\alpha,z} \underline{\gamma}_\alpha^T & \underline{0} & \underline{b}_x^T + h_{\alpha,x} \underline{\gamma}_\alpha^T \end{bmatrix} \tag{15}$$

It is noteworthy that this form of the discrete gradient operator is very useful since it allows each of the non-constant strain modes to be handled separately, so that the assumed strain field can be easily built. Moreover, it is easy to show that the $\underline{\gamma}_\alpha$ vectors that enter the expression of $\underline{\underline{B}}$ matrix verify the following orthogonality conditions:

$$\underline{\gamma}_\alpha^T \cdot \underline{x}_j = 0, \qquad \underline{\gamma}_\alpha^T \cdot \underline{h}_\beta = \delta_{\alpha\beta} \tag{16}$$

These properties will be useful in the subsequent hourglass stability analysis of the SHB8PS element.

2.3. Hourglass modes for the SHB8PS element

The hourglass modes of the SHB8PS element are analyzed following the approach given in Ref. [3]. For the SHB8PS element, these spurious modes are shown to originate in the particular position of the integration points (along a line). They are characterized by a vanishing energy, while inducing a non-zero strain. This pathological behaviour is explained by the difference between the kernel of the discrete and the continuous stiffness operators. It is recalled that the shell-like behaviour of the SHB8PS element is obtained by modifying its three-dimensional constitutive law to approach the plane stress conditions and by aligning the five integration points of the element along a particular direction, called the thickness. This reduced integration also aims to increase the computational efficiency and to avoid some shear locking phenomena in bending-dominated problems. Accordingly, the elastic stiffness is obtained by Gauss integration:

$$\underline{\underline{K}}_e = \int_{\Omega_e} \underline{\underline{B}}^T \cdot \underline{\underline{C}} \cdot \underline{\underline{B}}\, d\Omega = \sum_{I=1}^{5} \omega(\zeta_I) J(\zeta_I) \underline{\underline{B}}^T(\zeta_I) \cdot \underline{\underline{C}} \cdot \underline{\underline{B}}(\zeta_I) \tag{17}$$

where $J(\zeta_I)$ is the Jacobian of the transformation between the unit, reference configuration and the current configuration of an arbitrary hexahedron. Table 1 below gives the coordinates of the five integration points of the SHB8PS element, as well as the associated weights (the roots of the Gauss-Legendre polynomial):

Table 1: Coordinates and weights of the integration points.

	ξ	η	ζ	ω
P(1)	0	0	-0,91	0,24
P(2)	0	0	-0,54	0,48
P(3)	0	0	0	0,57
P(4)	0	0	0,54	0,48
P(5)	0	0	0,91	0,24

For the five Gauss points $(I = 1, ..., 5)$ listed in the above Table, with coordinates $\xi_I = \eta_I = 0,\ \zeta_I \neq 0,$ the terms $h_{\alpha,i}$ $(\alpha = 3, 4;\ i = 1, 2, 3)$ vanish. Consequently, the operator $\underline{\underline{B}}$ defined by Eqn. (15) reduces to $\underline{\underline{B}}_{12}$, where the sum on the index α only goes from 1 to 2:

$$\underline{\underline{B}}_{12} = \begin{bmatrix} \underline{b}^T + \sum_{\alpha=1}^{2} h_{\alpha,x} \underline{\gamma}_\alpha^T & \underline{0} & \underline{0} \\ \underline{0} & \underline{b}^T + \sum_{\alpha=1}^{2} h_{\alpha,y} \underline{\gamma}_\alpha^T & \underline{0} \\ \underline{0} & \underline{0} & \underline{b}^T + \sum_{\alpha=1}^{2} h_{\alpha,z} \underline{\gamma}_\alpha^T \\ \underline{b}^T + \sum_{\alpha=1}^{2} h_{\alpha,y} \underline{\gamma}_\alpha^T & \underline{b}^T + \sum_{\alpha=1}^{2} h_{\alpha,x} \underline{\gamma}_\alpha^T & \underline{0} \\ \underline{0} & \underline{b}^T + \sum_{\alpha=1,2} h_{\alpha,z} \underline{\gamma}_\alpha^T & \underline{b}^T + \sum_{\alpha=1}^{2} h_{\alpha,y} \underline{\gamma}_\alpha^T \\ \underline{b}^T + \sum_{\alpha=1}^{2} h_{\alpha,z} \underline{\gamma}_\alpha^T & \underline{0} & \underline{b}^T + \sum_{\alpha=1,2} h_{\alpha,x} \underline{\gamma}_\alpha^T \end{bmatrix} \tag{18}$$

In order to study the kernel of the stiffness matrix, a basis for the discretized displacements is built. Then, the reduced integration is shown to diminish the rank of the discrete stiffness. Indeed, according to Eqn. (17), the rank of the stiffness matrix $\underline{\underline{K}}_e$ is related to that of the $\underline{\underline{B}}$ matrix. In other words, one should seek the zero-strain modes $\underline{d}$ that verify at each Gauss point:

$$\underline{\underline{\nabla}}_s(\underline{u}) = \underline{\underline{B}}(\zeta_I) \cdot \underline{d} = \underline{0} \tag{19}$$

Using the expression (18) for the discrete gradient operator computed at the integration points and making use of the orthogonality relations (10) and (16), the kernel of the stiffness can be explicitly derived. This naturally reveals the six rigid body modes only found in the kernel of a fully integrated stiffness:

$$\begin{pmatrix} \underline{s} \\ \underline{0} \\ \underline{0} \end{pmatrix}, \begin{pmatrix} \underline{0} \\ \underline{s} \\ \underline{0} \end{pmatrix}, \begin{pmatrix} \underline{0} \\ \underline{0} \\ \underline{s} \end{pmatrix}, \begin{pmatrix} \underline{y} \\ -\underline{x} \\ \underline{0} \end{pmatrix}, \begin{pmatrix} \underline{z} \\ \underline{0} \\ -\underline{x} \end{pmatrix}, \begin{pmatrix} \underline{0} \\ \underline{z} \\ -\underline{y} \end{pmatrix} \tag{20}$$

The first three column vectors correspond to the translations along the Ox, Oy and Oz axes, respectively. The three remaining vectors refer to the rotations about the Oz, Oy and Ox axes, respectively.

In addition to these six rigid body modes, the following six vectors are also found in the kernel of the stiffness $\underline{\underline{K}}_e$:

$$\begin{pmatrix} \underline{h} \\ \underline{0} \\ \underline{0} \end{pmatrix}, \begin{pmatrix} \underline{0} \\ \underline{h} \\ \underline{0} \end{pmatrix}, \begin{pmatrix} \underline{0} \\ \underline{0} \\ \underline{h} \end{pmatrix}, \begin{pmatrix} \underline{h} \\ \underline{0} \\ \underline{0} \end{pmatrix}, \begin{pmatrix} \underline{0} \\ \underline{h} \\ \underline{0} \end{pmatrix}, \begin{pmatrix} \underline{0} \\ \underline{0} \\ \underline{h} \end{pmatrix} \tag{21}$$

The hourglass modes corresponding to Ox axis are shown in Fig. 2 for a hexahedron with a single integration point, located at the origin of the referential coordinate system. Similar modes are obtained for the Oy or Oz axes by axis permutation.

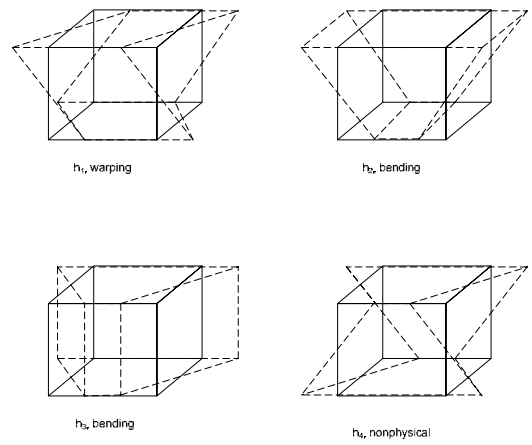

Figure 2: Hourglass modes in x-direction for a one-point quadrature hexahedron.

2.4. Stabilization and hourglass control

The control of the six hourglass modes of the SHB8PS element, as revealed by Eqn. (21), is achieved by adding a stabilization stiffness to the stiffness matrix $\underline{\underline{K}}_e$. This part is drawn from the approach given in Ref. [3]. The stabilization

forces are deduced in the same way. It is important to note that this stabilization part is treated independently from the assumed strain projection part, the later being intended to eliminate the locking phenomena. This projection technique will be applied in next section.

Let us start by decomposing the $\underline{\underline{B}}$ matrix into two parts as follows:

$$\underline{\underline{B}} = \underline{\underline{B}}_{12} + \underline{\underline{B}}_{34} \tag{22}$$

The first term in this additive decomposition is given by Eqn. (18). The second term $\underline{\underline{B}}_{34}$ is precisely the one that vanishes at the Gauss points. It is given by the following matrix form:

$$\underline{\underline{B}}_{34} = \begin{bmatrix} \sum_{\alpha=3}^{4} h_{\alpha,x}\underline{\gamma}_{\alpha}^{T} & \underline{0} & \underline{0} \\ \underline{0} & \sum_{\alpha=3}^{4} h_{\alpha,y}\underline{\gamma}_{\alpha}^{T} & \underline{0} \\ \underline{0} & \underline{0} & \sum_{\alpha=3}^{4} h_{\alpha,z}\underline{\gamma}_{\alpha}^{T} \\ \sum_{\alpha=3}^{4} h_{\alpha,y}\underline{\gamma}_{\alpha}^{T} & \sum_{\alpha=3}^{4} h_{\alpha,x}\underline{\gamma}_{\alpha}^{T} & \underline{0} \\ \underline{0} & \sum_{\alpha=3,4} h_{\alpha,z}\underline{\gamma}_{\alpha}^{T} & \sum_{\alpha=3}^{4} h_{\alpha,y}\underline{\gamma}_{\alpha}^{T} \\ \sum_{\alpha=3}^{4} h_{\alpha,z}\underline{\gamma}_{\alpha}^{T} & \underline{0} & \sum_{\alpha=3,4} h_{\alpha,x}\underline{\gamma}_{\alpha}^{T} \end{bmatrix} \tag{23}$$

In the standard displacement approach, the stiffness and internal forces are defined as:

$$\begin{aligned} \underline{\underline{K}}_{e} &= \int_{\Omega_e} \underline{\underline{B}}^{T} \cdot \underline{\underline{C}} \cdot \underline{\underline{B}}\, d\Omega \\ \underline{f}^{int} &= \int_{\Omega_e} \underline{\underline{B}}^{T} \cdot \underline{\sigma}\, d\Omega \end{aligned} \tag{24}$$

By introducing the additive decomposition (22) of the $\underline{\underline{B}}$ matrix, the stiffness matrix becomes:

$$\begin{aligned} \underline{\underline{K}}_{e} &= \int_{\Omega_e} \underline{\underline{B}}_{12}^{T} \cdot \underline{\underline{C}} \cdot \underline{\underline{B}}_{12}\, d\Omega + \int_{\Omega_e} \underline{\underline{B}}_{12}^{T} \cdot \underline{\underline{C}} \cdot \underline{\underline{B}}_{34}\, d\Omega \\ &+ \int_{\Omega_e} \underline{\underline{B}}_{34}^{T} \cdot \underline{\underline{C}} \cdot \underline{\underline{B}}_{12}\, d\Omega + \int_{\Omega_e} \underline{\underline{B}}_{34}^{T} \cdot \underline{\underline{C}} \cdot \underline{\underline{B}}_{34}\, d\Omega \end{aligned} \tag{25}$$

which can be simply written as:

$$\underline{\underline{K}}_{e} = \underline{\underline{K}}_{12} + \underline{\underline{K}}_{STAB} \tag{26}$$

The first term, $\underline{\underline{K}}_{12}$, is the only one taken into account when the stiffness is evaluated at the Gauss points as defined above. It reads:

$$\underline{\underline{K}}_{12} = \int_{\Omega_e} \underline{\underline{B}}_{12}^{T} \cdot \underline{\underline{C}} \cdot \underline{\underline{B}}_{12}\, d\Omega = \sum_{I=1}^{5} \omega(\zeta_I) J(\zeta_I) \underline{\underline{B}}_{12}^{T}(\zeta_I) \cdot \underline{\underline{C}} \cdot \underline{\underline{B}}_{12}(\zeta_I) \tag{27}$$

The second term, $\underline{\underline{K}}_{STAB}$, represents the stabilization stiffness since it vanishes if evaluated at the Gauss points:

$$\underline{\underline{K}}_{STAB} = \int_{\Omega_e} \underline{\underline{B}}_{12}^{T} \cdot \underline{\underline{C}} \cdot \underline{\underline{B}}_{34}\, d\Omega + \int_{\Omega_e} \underline{\underline{B}}_{34}^{T} \cdot \underline{\underline{C}} \cdot \underline{\underline{B}}_{12}\, d\Omega + \int_{\Omega_e} \underline{\underline{B}}_{34}^{T} \cdot \underline{\underline{C}} \cdot \underline{\underline{B}}_{34}\, d\Omega \tag{28}$$

In a similar way, the internal forces of the element can be written as:

$$\underline{f}^{int} = \underline{f}_{12}^{int} + \underline{f}^{STAB} \tag{29}$$

The first term, $\underline{f}_{12}^{int}$, is the only one taken into account when the forces are evaluated at the Gauss points:

$$\underline{f}_{12}^{int} = \int_{\Omega_e} \underline{\underline{B}}_{12}^{T} \cdot \underline{\sigma}\, d\Omega = \sum_{I=1}^{5} \omega(\zeta_I) J(\zeta_I) \underline{\underline{B}}_{12}^{T}(\zeta_I) \cdot \underline{\sigma}(\zeta_I) \tag{30}$$

The second term $\underline{f}^{STAB}$ of Eqn. (29) represents the stabilization forces and should be consistently calculated according to the stabilization stiffness given by Eqn. (28).

Since the stabilization stiffness and forces cannot be calculated properly at the integration points, we will calculate them in the co-rotational coordinate system proposed in Ref. [3], in order to prevent the hourglass mode phenomena. An intermediate stage for this approach consists in the projection of $\underline{\underline{B}}$ onto a $\overline{\underline{\underline{B}}}$ matrix, in order to eliminate the remaining locking problems.

2.5. Assumed strain field and orthogonal projection

The discrete gradient operator is projected onto an appropriate sub-space in order to eliminate shear and membrane locking. This projection technique can be derived from the formalism of the assumed strain method. It is also shown that this approach can be justified within the framework of the Hu-Washizu nonlinear mixed variational principle (see for instance Ref. [9]). Indeed, this variational principle reads:

$$\delta\pi(\underline{v}, \dot{\overline{\underline{\underline{\varepsilon}}}}, \overline{\underline{\underline{\sigma}}}) = \int_{\Omega_e} \delta\dot{\overline{\underline{\underline{\varepsilon}}}}^{T} \cdot \underline{\underline{\sigma}}\, d\Omega + \delta \int_{\Omega_e} \overline{\underline{\underline{\sigma}}}^{T} \cdot \left(\underline{\underline{\nabla}}_s(\underline{v}) - \dot{\overline{\underline{\underline{\varepsilon}}}} \right) d\Omega - \delta\dot{\underline{d}}^{T} \cdot \underline{f}^{ext} = 0 \tag{31}$$

where δ denotes a variation, $\underline{v}$ the velocity field, $\dot{\overline{\underline{\underline{\varepsilon}}}}$ the assumed strain rate, $\overline{\underline{\underline{\sigma}}}$ the interpolated stress, $\underline{\underline{\sigma}}$ the stress evaluated by the constitutive law, $\dot{\underline{d}}$ the nodal velocities, $\underline{f}^{ext}$ the external nodal forces and $\underline{\underline{\nabla}}_s(\underline{v})$ the symmetric part of the velocity gradient. The assumed strain formulation used to construct the SHB8PS element is a simplified form of the Hu-Washizu variational principle as described in Ref. [14]. In this simplified form, the interpolated stress is chosen to be orthogonal to the difference between the symmetric part of the velocity gradient and the assumed strain rate. Consequently, the second term of Eqn. (31) vanishes and one obtains:

$$\delta\pi(\underline{v}, \dot{\overline{\underline{\underline{\varepsilon}}}}) = \int_{\Omega_e} \delta\dot{\overline{\underline{\underline{\varepsilon}}}}^{T} \cdot \underline{\underline{\sigma}}\, d\Omega - \delta\dot{\underline{d}}^{T} \cdot \underline{f}^{ext} = 0 \tag{32}$$

In this form, the variational principle is independent of the stress interpolation, since the interpolated stress is eliminated and does not need to be defined. The discrete equations then only require the interpolation of the velocity and of the assumed strain field. The assumed strain rate $\dot{\overline{\underline{\underline{\varepsilon}}}}$ is expressed in terms of a $\overline{\underline{\underline{B}}}$ matrix, projected starting from the classical discrete gradient $\underline{\underline{B}}$ defined by Eqn. (14) and (15):

$$\dot{\overline{\underline{\underline{\varepsilon}}}}(x,t) = \overline{\underline{\underline{B}}}(x) \cdot \dot{\underline{d}}(t) \tag{33}$$

Once this expression is replaced in the variational principle (32), the new expressions for the elastic stiffness and internal forces are obtained:

$$\underline{\underline{K}}_e = \int_{\Omega_e} \underline{\underline{\overline{B}}}^T \cdot \underline{\underline{C}} \cdot \underline{\underline{\overline{B}}}\, d\Omega \quad , \quad \underline{f}^{int} = \int_{\Omega_e} \underline{\underline{\overline{B}}}^T \cdot \underline{\sigma}(\underline{\underline{\dot{\overline{\varepsilon}}}})\, d\Omega \tag{34}$$

Before defining the projected $\underline{\underline{\overline{B}}}$ operator, let us replace in the previous equations the Hallquist form of the $\underline{b}$ vectors, Eqn. (9), by the mean form $\hat{\underline{b}}$ from (Ref. [6]):

$$\hat{\underline{b}}^T = \frac{1}{\Omega_e} \int_{\Omega_e} \underline{N}_{,i}(\xi,\eta,\zeta) d\Omega, \quad i = 1,2,3 \quad \textit{Mean value form} \tag{35}$$

Accordingly, the vectors $\underline{\gamma}_\alpha$ are replaced by the vectors $\hat{\underline{\gamma}}_\alpha$ defined as:

$$\hat{\underline{\gamma}}_\alpha = \frac{1}{8}\left[\underline{h}_\alpha - \sum_{j=1}^{3} (\underline{h}_\alpha^T \cdot \underline{x}_j) \hat{\underline{b}}_j \right] \tag{36}$$

Finally, the $\underline{\underline{B}}$ matrix, defined by Eqn. (15), is replaced by the $\hat{\underline{\underline{B}}}$ operator defined by:

$$\hat{\underline{\underline{B}}} = \begin{bmatrix} \hat{\underline{b}}_1^T + h_{\alpha,x}\hat{\underline{\gamma}}_\alpha^T & \underline{0} & \underline{0} \\ \underline{0} & \hat{\underline{b}}_2^T + h_{\alpha,y}\hat{\underline{\gamma}}_\alpha^T & \underline{0} \\ \underline{0} & \underline{0} & \hat{\underline{b}}_3^T + h_{\alpha,z}\hat{\underline{\gamma}}_\alpha^T \\ \hat{\underline{b}}_2^T + h_{\alpha,y}\hat{\underline{\gamma}}_\alpha^T & \hat{\underline{b}}_1^T + h_{\alpha,x}\hat{\underline{\gamma}}_\alpha^T & \underline{0} \\ \underline{0} & \hat{\underline{b}}_3^T + h_{\alpha,z}\hat{\underline{\gamma}}_\alpha^T & \hat{\underline{b}}_2^T + h_{\alpha,y}\hat{\underline{\gamma}}_\alpha^T \\ \hat{\underline{b}}_3^T + h_{\alpha,z}\hat{\underline{\gamma}}_\alpha^T & \underline{0} & \hat{\underline{b}}_1^T + h_{\alpha,x}\hat{\underline{\gamma}}_\alpha^T \end{bmatrix} \tag{37}$$

The approach developed earlier still applies, as well as the expressions of the stabilization stiffness and internal forces, if the same additive decomposition is adopted:

$$\hat{\underline{\underline{B}}} = \hat{\underline{\underline{B}}}_{12} + \hat{\underline{\underline{B}}}_{34} \tag{38}$$

It is noteworthy that in the former version of the SHB8PS element, the Hallquist forms $\underline{b}$ have been replaced with the mean expressions $\hat{\underline{b}}$ of Flanagan-Belytschko only in the stabilization terms $\hat{\underline{\underline{B}}}_{34}$ and thus $\underline{\underline{K}}_{STAB}$.

It is also important to note that the two forms $\underline{b}$ and $\hat{\underline{b}}$ have been tested on a large number of test problems and that Flanagan-Belytschko's mean form performed better in all cases. Its better convergence is even more dramatic when a few, highly distorted elements are used. Similar results have been found in Ref. [3] with an assumed strain, eight-node solid element with one-point quadrature.

At this stage, one can project the $\hat{\underline{\underline{B}}}$ operator from Eqn. (38) onto a $\overline{\hat{\underline{\underline{B}}}}$ operator such as:

$$\overline{\hat{\underline{\underline{B}}}} = \hat{\underline{\underline{B}}}_{12} + \overline{\hat{\underline{\underline{B}}}}_{34} \tag{39}$$

It is clear that only the second term $\hat{\underline{\underline{B}}}_{34}$ from Eqn. (38) is projected; the first term $\hat{\underline{\underline{B}}}_{12}$ remains unchanged and is given by Eqn. (18) where the vectors $\underline{b}$ are replaced by $\hat{\underline{b}}$. The operator $\hat{\underline{\underline{B}}}_{34}$ is projected onto $\overline{\hat{\underline{\underline{B}}}}_{34}$ given by:

$$\overline{\hat{\underline{\underline{B}}}}_{34} = \begin{bmatrix} \sum_{\alpha=3}^{4} h_{\alpha,x}\hat{\underline{\gamma}}_\alpha^T & \underline{0} & \underline{0} \\ \underline{0} & \sum_{\alpha=3}^{4} h_{\alpha,y}\hat{\underline{\gamma}}_\alpha^T & \underline{0} \\ \underline{0} & \underline{0} & h_{3,z}\hat{\underline{\gamma}}_3^T \\ \underline{0} & \underline{0} & \underline{0} \\ \underline{0} & \underline{0} & \underline{0} \\ \underline{0} & \underline{0} & h_{4,x}\hat{\underline{\gamma}}_4^T \end{bmatrix} \tag{40}$$

The elastic stiffness is then given by Eqn. (26) as the sum of the following two contributions:

$$\underline{\underline{K}}_{12} = \int_{\Omega_e} \hat{\underline{\underline{B}}}_{12}^T \cdot \underline{\underline{C}} \cdot \hat{\underline{\underline{B}}}_{12}\, d\Omega = \sum_{I=1}^{5} \omega(\zeta_I) J(\zeta_I) \hat{\underline{\underline{B}}}_{12}^{\ T}(\zeta_I) \cdot \underline{\underline{C}} \cdot \hat{\underline{\underline{B}}}_{12}(\zeta_I) \tag{41}$$

$$\underline{\underline{K}}_{STAB} = \int_{\Omega_e} \hat{\underline{\underline{B}}}_{12}^T \cdot \underline{\underline{C}} \cdot \overline{\hat{\underline{\underline{B}}}}_{34}\, d\Omega + \int_{\Omega_e} \overline{\hat{\underline{\underline{B}}}}_{34}^T \cdot \underline{\underline{C}} \cdot \hat{\underline{\underline{B}}}_{12}\, d\Omega + \int_{\Omega_e} \overline{\hat{\underline{\underline{B}}}}_{34}^T \cdot \underline{\underline{C}} \cdot \overline{\hat{\underline{\underline{B}}}}_{34}\, d\Omega \tag{42}$$

The stabilization stiffness, Eqn. (42), is calculated in a co-rotational coordinate system (see Ref. [3]). This orthogonal co-rotational system that is embedded in the element and rotates with the element is chosen to be aligned with the referential coordinate system. This choice is justified here by the rotation extracted from the polar decomposition of the transformation gradient (Refs. [1], [2]). As noticed in Ref. [3], such a co-rotational approach has numerous advantages: simplified expressions for the above stiffness matrix, whose first two terms vanish; more effective treatment of the shear locking in this frame; the co-rotational system assures a frame-invariant element.

The main equations defining the chosen co-rotational coordinate system are given hereafter. First, the components of the column vectors forming the rotation matrix are computed:

$$a_{1i} = \underline{\Lambda}_1^T \cdot \underline{x} \quad , \quad a_{2i} = \underline{\Lambda}_2^T \cdot \underline{x} \quad , \quad i = 1,2,3 \tag{43}$$

with:

$$\begin{cases} \underline{\Lambda}_1^T = (-1,1,1,-1,-1,1,1,-1) \\ \underline{\Lambda}_2^T = (-1,-1,1,1,-1,-1,1,1) \\ \underline{\Lambda}_3^T = (-1,-1,-1,-1,1,1,1,1) \end{cases} \tag{44}$$

Then, the correction term $\underline{a}_2$ is calculated so that the orthogonality relation $\underline{a}_1^T \cdot \left(\underline{a}_3 + \underline{a}_2 \right) = 0$ is verified:

$$\underline{a}_2 = -\frac{\underline{a}_1^T \cdot \underline{a}_3}{\underline{a}_1^T \cdot \underline{a}_1}\, \underline{a}_1 \tag{45}$$

The third base vector $\underline{a}_3$ is then obtained by the cross-product:

$$\underline{a}_3 = \underline{a}_1 \wedge \left(\underline{a}_3 + \underline{a}_2 \right) \tag{46}$$

The rotation matrix $\underline{\underline{R}}$ that maps a vector in the global coordinate system to the co-rotational system is finally given, after normalization, by:

$$R_{1i} = \frac{a_{1i}}{\|\underline{a}_1\|} \quad , \quad R_{2i} = \frac{a_{2i} + a_{ci}}{\|\underline{a}_2 + \underline{a}_c\|} \quad , \quad R_{3i} = \frac{a_{3i}}{\|\underline{a}_3\|} \quad , \quad i = 1, 2, 3 \tag{47}$$

The stabilization terms (stabilization stiffness and internal forces, Eqn. (42)) are computed in this co-rotational coordinate system, where several terms simplify. Indeed, in this co-rotational system one obtains:

$$\begin{cases} \int_{\Omega_e} h_{i,j} \, d\Omega = 0 \\ H_{ii} = \int_{\Omega_e} \left(h_{j,i}\right)^2 d\Omega = \int_{\Omega_e} \left(h_{k,i}\right)^2 d\Omega = 3\int_{\Omega_e} \left(h_{4,i}\right)^2 d\Omega = \frac{1}{3}\frac{\left(\underline{\Lambda}_j^T \cdot \underline{x}_j\right)\left(\underline{\Lambda}_k^T \cdot \underline{x}_k\right)}{\left(\underline{\Lambda}_i^T \cdot \underline{x}_i\right)} \\ H_{ij} = \int_{\Omega_e} h_{i,j} h_{j,i} \, d\Omega = \frac{1}{3} \underline{\Lambda}_k^T \cdot \underline{x}_k \end{cases} \tag{48}$$

In these last formulas, there is no sum on repeated subscripts. Moreover, the subscripts i, j and k in the expressions of H_{ii} and H_{ij} are two by two distinct and take the values 1, 2 and 3 with all of the possible permutations. Using these explicit expressions, the stabilization stiffness given in Eqn. (42) is obtained completely analytically in this co-rotational system as:

$$\underline{\underline{K}}_{STAB} = \begin{bmatrix} \underline{\underline{k}}_{11} & \underline{\underline{k}}_{12} & \underline{\underline{k}}_{13} \\ \underline{\underline{k}}_{21} & \underline{\underline{k}}_{22} & \underline{\underline{k}}_{23} \\ \underline{\underline{k}}_{31} & \underline{\underline{k}}_{32} & \underline{\underline{k}}_{33} \end{bmatrix} \tag{49}$$

where the 8 x 8 matrices $\underline{\underline{k}}_{ij}$ are given by:

$$\begin{cases} \underline{\underline{k}}_{11} = (\overline{\lambda} + 2\mu) H_{11} \left[\hat{\underline{\gamma}}_3 \hat{\underline{\gamma}}_3^T + \frac{1}{3} \hat{\underline{\gamma}}_4 \hat{\underline{\gamma}}_4^T \right] \\ \underline{\underline{k}}_{22} = (\overline{\lambda} + 2\mu) H_{22} \left[\hat{\underline{\gamma}}_3 \hat{\underline{\gamma}}_3^T + \frac{1}{3} \hat{\underline{\gamma}}_4 \hat{\underline{\gamma}}_4^T \right] \\ \underline{\underline{k}}_{33} = \mu H_{11} \frac{1}{3} \hat{\underline{\gamma}}_4 \hat{\underline{\gamma}}_4^T \\ \underline{\underline{k}}_{ij} = \underline{\underline{0}} \quad , \quad i \neq j \end{cases} \tag{50}$$

Note that an improved, plane-stress type constitutive law is adopted for the SHB8PS element. This specific law is given by:

$$\underline{\underline{C}} = \begin{bmatrix} \overline{\lambda} + 2\mu & \overline{\lambda} & 0 & 0 & 0 & 0 \\ \overline{\lambda} & \overline{\lambda} + 2\mu & 0 & 0 & 0 & 0 \\ 0 & 0 & E & 0 & 0 & 0 \\ 0 & 0 & 0 & \mu & 0 & 0 \\ 0 & 0 & 0 & 0 & \mu & 0 \\ 0 & 0 & 0 & 0 & 0 & \mu \end{bmatrix} \tag{51}$$

$$\mu = \frac{E}{2(1+\nu)} \qquad \overline{\lambda} = \frac{E\nu}{1-\nu^2}$$

On one hand, the choice of this constitutive matrix avoids locking encountered with a full three-dimensional law and, on the other hand, allows for the deformation energy associated to the strains normal to the mean surface of the element to be taken into account.

For the computation of the internal forces of the element, the same approach is adopted (Refs. [1], [2]). The additive decomposition (39) and the projection (40) allow for the calculation of the stabilization forces:

$$\underline{f}^{int} = \sum_{I=1}^{5} \omega(\zeta_I) J(\zeta_I) \hat{\underline{\underline{B}}}_{12}^T(\zeta_I) \cdot \underline{\sigma}(\zeta_I) + \underline{f}^{STAB} \tag{52}$$

where:

$$\underline{f}^{STAB} = \begin{pmatrix} \underline{f}_1^{STAB} \\ \underline{f}_2^{STAB} \\ \underline{f}_3^{STAB} \end{pmatrix} \tag{53}$$

and:

$$\underline{f}_i^{STAB} = \sum_{\alpha=3}^{4} Q_{i\alpha} \hat{\underline{\gamma}}_\alpha \quad , \quad i = 1, 2, 3 \tag{54}$$

The $Q_{i\alpha}$, called generalized stresses and entering the expressions of the stabilization forces, are related to the so-called generalized strains $q_{i\alpha}$ by the following incremental equations:

$$\begin{cases} \dot{Q}_{13} = (\overline{\lambda} + 2\mu) H_{11} \dot{q}_{13} \\ \dot{Q}_{14} = \frac{1}{3}(\overline{\lambda} + 2\mu) H_{11} \dot{q}_{14} \\ \dot{Q}_{23} = (\overline{\lambda} + 2\mu) H_{22} \dot{q}_{23} \\ \dot{Q}_{24} = \frac{1}{3}(\overline{\lambda} + 2\mu) H_{22} \dot{q}_{24} \\ \dot{Q}_{33} = 0 \\ \dot{Q}_{34} = \frac{1}{3} \mu H_{11} \dot{q}_{34} \end{cases} \tag{55}$$

The generalized strain rates $\dot{q}_{i\alpha}$ are given by:

$$\dot{q}_{i\alpha} = \hat{\underline{\gamma}}_\alpha^T \cdot \dot{\underline{d}}_i \quad , \quad i = 1, 2, 3 \quad , \quad \alpha = 3, 4 \tag{56}$$

The previous expressions for the stabilization stiffness and forces hold for an elastic behaviour. In the case of elastic-plastic behaviour, the Young's modulus E is replaced by the mean tangent modulus (i.e. the average of the tangent moduli at the five Gauss points across the thickness). This choice avoids the response to be too stiff, which is the case with a purely elastic hourglass stabilization. Thus this leads to an adaptive element provided with a stabilization that automatically adjusts to the physical situation of the element: elastic or elastic-plastic.

3. Numerical results

In order to validate the new version of the SHB8PS element, its performances have been tested, based on the analysis of a variety of linear and nonlinear benchmark problems frequently used in the literature. For each test problem, the results were compared to the reference solutions and, on the other hand, to those given by the previous version of the SHB8PS element (Ref. [10]). Note that several projections have been formulated in this study and extensively tested over a wide range of benchmark problems. The retained projection that is presented here is the one that showed the best convergence and exhibited no transverse shear and membrane locking phenomena. This projection improved the former version of the SHB8PS element in all cases and especially in the test of the pinched hemispherical shell where the improvement is significant.

3.1. *Pinched hemispherical shell*

This test has become very popular and has been used by many authors (see Ref. [13]). It is very severe since the transverse shear and membrane locking phenomena are very important and emphasized by the problem geometry (distorted, skewed elements). As reported by many authors, in this doubly-curved shell problem, the membrane locking is much more severe than the shear locking. Figure 3 shows the geometry, loading and boundary conditions for this problem.

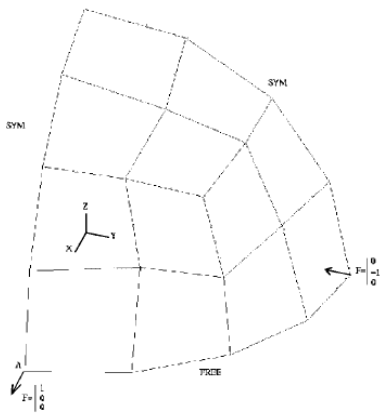

Figure 3: Schematic of hemispherical shell.

The radius is R=10, the thickness is t=0.04, the Young modulus is E=6.825×10^7 and the Poisson's ratio is ν=0.3. Using the symmetry of the problem (i.e. planes (XZ) and (YZ)), only a quarter of the hemisphere is meshed using a single element through the thickness and with two unit loads along directions Ox and Oy. Except for the symmetry, the boundary conditions are free; nevertheless, the displacement of one point in the z-direction is fixed in order to prevent rigid body motions. According to the reference solution (Ref. [13]), the radial displacement at the load point A along the x-direction equals 0.0924 (see Fig. 3). The convergence results are reported in Tab. 2 in terms of the normalized displacement at the load point in the x-direction. The new version of the SHB8PS element is compared to the former one and to the three elements HEX8, HEXDS and H8-ct-cp. The HEX8 element is the standard, eight-node, full integration solid element (eight Gauss points). The HEXDS element is an eight-node, four-point quadrature solid element (see Ref. [12]). The H8-ct-cp element was developed in Ref. [11]. Table 2 shows that the new version of the SHB8PS element provides an excellent convergence and shows no locking.

Table 2: Normalized displacement at the load point.

Number of elements	SHB8PS previous version	HEX8	HEXDS	H8-ct-cp	SHB8PS new version
	Ux/Uref	Ux/Uref	Ux/Uref	Ux/Uref	Ux/Uref
12	0.0629	0.0005		0.05	0.8645
27	0.0474	0.0011			1.0155
48	0.1660	0.0023	0.408	0.35	1.0098
75	0.2252	0.0030	0.512	0.58	1.0096
192	0.6332	0.0076	0.701	0.95	1.0008
363	0.8592	0.0140	0.800		1.0006
768	0.9651	0.0287			1.0006
1462	0.9910	0.0520			1.0009

3.2. *Pullout of an open-ended cylindrical shell*

This nonlinear test is severe and has been studied by several authors. Figure 4 shows the geometry, loading, boundary conditions as well as the material properties for this open-ended cylindrical shell pulled by a pair of radial forces.

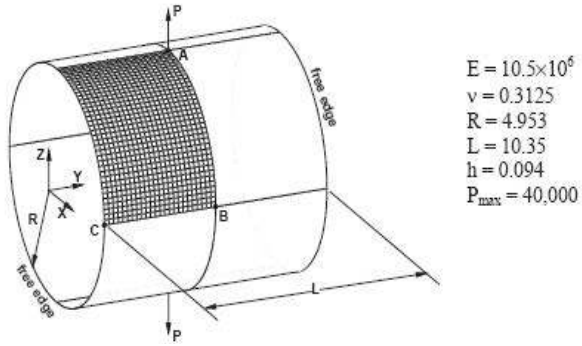

Figure 4: Geometry, loading and material properties.

Using the symmetry of the problem, only one-eighth of the shell is meshed with $24 \times 36 \times 1$ elements as in Ref. [15]. The reference solution is obtained from Ref. [15] which uses the S4R shell element in the finite element code Abaqus. Figure 5 plots the radial deflections at points A, B and C against the applied load.

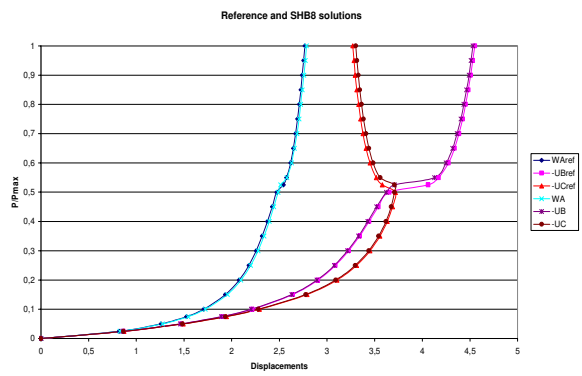

Figure 5: Load-deflection curves at points A, B and C: reference solution and numerical results obtained with the SHB8PS.

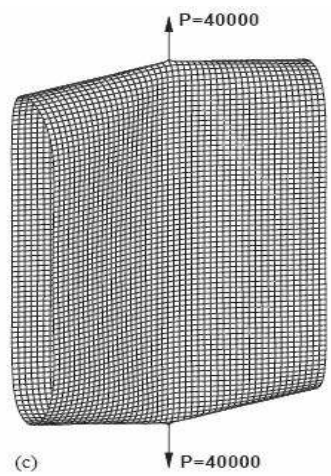

Figure 6: Deformed $24 \times 36 \times 1$ mesh under the maximum load.

It is noteworthy that this problem involves large displacements and rotations allowing the new version of the SHB8PS to be tested in nonlinear situations. The results given by this version of the SHB8PS are very close to those of the reference solution (Ref. [15]). A snap-through phenomenon occurs also at a certain critical load. This snap-through instability can be clearly observed in Fig. 5 corresponding to a change in displacement direction of point C, and also in Fig. 6 showing the deformed mesh for the cylindrical shell under maximum load of $P = 40000$.

3.3. Arch subjected to inclined load

An inclined force is applied at the center of the 90° arch, leading to unsymmetrical buckling (limit point). This test problem has been studied by several authors; we will compare our results with the reference solution given in Ref. [8]. Figure 7 shows the geometry where the two straight edges are simply supported, whereas the curved edges are free.

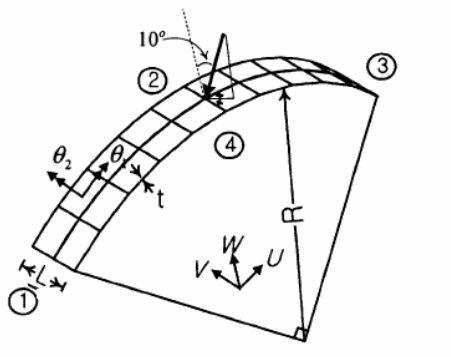

Figure 7: Geometry of the 90° arch subjected to inclined force.

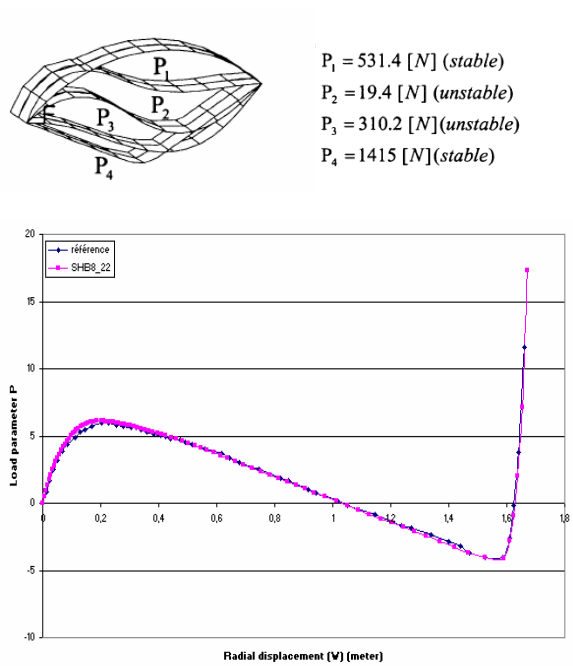

Figure 8: Load against radial-displacement at the load point: reference solution and numerical results obtained with a mesh of $20 \times 8 \times 1$ SHB8PS elements.

The geometrical dimensions and material properties are: $R = 2.54\,\text{m}$, $L = 0.504\,\text{m}$, $t = 0.0127\,\text{m}$; $E = 3.105\,\text{GPa}$, $\nu = 0.3$. The applied force uses a load parameter λ such that: $P = 100\lambda$ [N]; it is inclined of 10° with respect to Z axis and the in-plane inclination is 45°. Several meshes have been tested; Fig. 8 portrays the results obtained with a $20 \times 8 \times 1$ mesh and shows very good agreement with the reference solution. As shown by the successive states of the arch (Fig. 8), the pre-buckling is nonlinear and stable whereas the post-buckling is asymmetric and instable. The Riks' continuation method (arc length technique) has been used to follow the path after the limit point.

4. Discussion and conclusions

A new formulation of the solid-shell element SHB8PS has been developed and implemented into the implicit, nonlinear finite element code Stanlax-INCA. This new version has been evaluated, based on a variety of popular linear and nonlinear benchmark problems frequently used in the literature. Let us recall that this solid-shell element is based on a purely three-dimensional formulation (eight-node hexahedron and only three translational degrees of freedom per node). A reduced integration is used to improve the computational efficiency and an effective stabilization is built for hourglass mode control. Five integration points are used along a particular chosen direction designated as the "thickness", allowing accurate modelling of bending-dominated structural problems using only a single element through the thickness. Moreover, we demonstrate that the projection adopted in this new formulation of the element better eliminates the various numerical locking phenomena. Indeed, the excellent efficiency and convergence properties of the element have been clearly shown through numerous tests. All these tests prove that there is no residual locking (membrane, shear). In particular, the improvement is significant in the pinched hemispherical shell problem, where the amount of locking observed in the former version has been eliminated.

5. References

[1] Abed-Meraim, F. and Combescure, A., SHB8PS a new intelligent assumed strain continuum mechanics shell element for impact analysis on a rotating body, *First M.I.T. Conference on Comput. Fluid and Solid Mechanics*, 12-15 June, U.S.A., 2001.

[2] Abed-Meraim, F. and Combescure, A., SHB8PS- a new adaptive, assumed-strain continuum mechanics shell element for impact analysis, *Computers & Structures*, Vol. 80, pp. 791-803, 2002.

[3] Belytschko, T. and Bindeman, L.P., Assumed strain stabilization of the eight node hexahedral element, *Computer Methods in Applied Mechanics and Engineering,* Vol. 105, pp. 225-260, 1993.

[4] Belytschko, T., Ong, J.S.-J., Liu, W.K. and Kennedy, J.M., Hourglass control in linear and nonlinear problems, *Computer Methods in Applied Mechanics and Engineering,* Vol. 43, pp. 251-276, 1984.

[5] Chen, Y.-I. and Wu, G.-Y., A mixed 8-node hexahedral element based on the Hu-Washizu principle and the field extrapolation technique, *Structural Engineering and Mechanics*, Vol. 17, No. 1, pp. 113-140, 2004.

[6] Flanagan, D.P. and Belytschko, T., A uniform strain hexahedron and quadrilateral with orthogonal hourglass

control, *International Journal for Numerical Methods and Engineering*, Vol. 17, pp. 679-706, 1981.

[7] Hallquist, J.O., *Theoretical manual for DYNA3D,* UC1D-19401 Lawrence Livermore National Lab., University of California, 1983.

[8] Kim, J.H. and Kim, Y.H., A predictor-corrector method for structural nonlinear analysis, *Computer Methods in Applied Mechanics and Engineering*, Vol. 191, pp. 959-974, 2001.

[9] Korelec, J. and Wriggers, P., Consistent gradient formulation for a stable enhanced strain method for large deformations, *Engineering Computations*, Vol. 13, pp. 103-123, 1996.

[10] Legay, A. and Combescure, A., Elastoplastic stability analysis of shells using the physically stabilized finite element SHB8PS, *International Journal for Numerical Methods and Engineering*, Vol. 57, pp. 1299-1322, 2003.

[11]Lemosse, D., *Eléments finis iso-paramétriques tridimensionnels pour l'étude des structures minces*, PhD Thesis, Ecole Doctorale SPMI/INSA-Rouen, 2000.

[12] Liu, W.K., Guo, Y., Tang, S. and Belytschko, T., A multiple-quadrature eight-node hexahedral finite element for large deformation elastoplastic analysis, *Comput. Meth. in Applied Mech. and Engng*, Vol. 154, pp. 69-132, 1998.

[13] MacNeal, R.H. and Harder, R.L., A proposed standard set of problems to test finite element accuracy, *Finite Elements in Analysis and Design,* Vol. 1, pp. 3-20, 1985.

[14] Simo, J.C. and Hughes, T.J.R., On the variational foundations of assumed strain methods, *Journal of Applied Mechanics,* ASME, Vol. 53, pp. 51-54, 1986.

[15] Sze, K.Y., Liu, X.H. and Lo, S.H., Popular benchmark problems for geometric nonlinear analysis of shells, *Finite Elements in Analysis and Design*, Vol. 40, pp. 1551-1569, 2004.

[16] Sze, K.Y. and Yao, L.Q., A hybrid stress ANS solid-shell element and its generalization for smart structure modelling. Part I-solid-shell element formulation, *International Journal for Num. Methods and Engng*, Vol. 48, pp. 545-564, 2000.